Effect of pH on the Binding of Sodium, Lysine, and Arginine Counterions to l-Undecyl Leucinate Micelles

Corbin Lewis, Burgoyne H. Hughes, Mariela Vasquez, Alyssa M. Wall, Victoria L. Northrup, Tyler J. Witzleb, Eugene J. Billiot, et al.

Journal of Surfactants and Detergents

ISSN 1097-3958 Volume 19 Number 6

J Surfact Deterg (2016) 19:1175-1188 DOI 10.1007/s11743-016-1875-y





Your article is protected by copyright and all rights are held exclusively by AOCS. This eoffprint is for personal use only and shall not be self-archived in electronic repositories. If you wish to self-archive your article, please use the accepted manuscript version for posting on your own website. You may further deposit the accepted manuscript version in any repository, provided it is only made publicly available 12 months after official publication or later and provided acknowledgement is given to the original source of publication and a link is inserted to the published article on Springer's website. The link must be accompanied by the following text: "The final publication is available at link.springer.com".



ORIGINAL ARTICLE



Effect of pH on the Binding of Sodium, Lysine, and Arginine Counterions to L-Undecyl Leucinate Micelles

Corbin Lewis¹ · Burgoyne H. Hughes² · Mariela Vasquez¹ · Alyssa M. Wall² · Victoria L. Northrup² · Tyler J. Witzleb² · Eugene J. Billiot¹ · Yayin Fang³ · Fereshteh H. Billiot¹ · Kevin F. Morris²

Received: 20 May 2016/Accepted: 6 September 2016/Published online: 20 September 2016 © AOCS 2016

Abstract Micelle formation by the amino acid-based surfactant undecylenyl L-leucine was investigated as a function of solution pH with NMR, dynamic light scattering, and fluorescence spectroscopy. NMR and dynamic light scattering showed that 50 mM undecylenyl L-leucine and 50 mM NaHCO₃ solutions contained micelles approximately 20 Å in diameter and that micelle radius and the mole fraction of surfactant molecules associated with micelles changed very little with solution pH. The binding of the amino acids arginine and lysine to the anionic micelles was also investigated from pH 7.0 to 11.5. Below pH 9.0, the mole fraction of arginine cations bound to the micelles was approximately 0.4. Above pH 9.0, the arginine counterions became zwitterionic, and the mole fraction of bound arginine molecules decreased steadily to less than 0.1 at pH 11. When arginine dissociated from the micelles, their radii decreased from 14 to 10 Å. Similar behavior was observed with lysine; however, when lysine dissociated from the micelle surface, little change in micelle radius was observed. Two-dimensional NMR experiments suggested that below pH 9.0, L-arginine bound perpendicular to the micelle surface primarily though its side chain amine while L-lysine bound parallel to the surface through both of its amine functional groups. Finally, the rate at which the amide protons on the surfactant headgoup exchanged with solvent was investigated with NMR spectroscopy. The exchange reaction was faster in solutions containing only surfactant monomers and slower when the surfactants were in micellar form and the headgoup amide protons were less exposed to solvent.

Keywords Amino acid surfactant · Micelle · Counterion · **NMR**

Abbreviations

CMC Critical micelle concentration DLS Dynamic light scattering **HPLC** High-performance liquid chromatography **NMR** Nuclear magnetic resonance

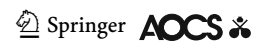
ROESY Rotating frame Overhauser enhancement

> spectroscopy Tetramethylsilane

TMS und-Leu Undecylenyl L-leucine

Introduction

Surfactants are widely used, versatile compounds, with applications in science, medicine, agriculture, oil recovery, and consumer products [1–10]. These surface-active compounds are amphiphilic because they contain both polar and non-polar regions. The micellar association of amphiphilic molecules in water is the result of a delicate balance between hydrophobic and hydrophilic forces. In micelles, the polar head groups align at the micelle-water interface, while the non-polar hydrocarbon chains interact with one another in the micelle core [11-13]. This micelle structure is dynamic, with surfactant molecules free to



Kevin F. Morris kmorris@carthage.edu

Department of Physical and Environmental Sciences, Texas A&M University-Corpus Christi, 6300 Ocean Drive, Corpus Christi, TX 78412, USA

Department of Chemistry, Carthage College, 2001 Alford Park Drive, Kenosha, WI 53140, USA

Department of Biochemistry and Molecular Biology, Howard University College of Medicine, Howard University, 520 W Street NW, Washington, DC 20059, USA

exchange between the micelle and free solution. Micelle formation occurs only when the concentration of surfactant molecules in solution exceeds the critical micelle concentration (CMC). Above the CMC, van der Waals interactions between the surfactants' hydrocarbon tails favor micellization, while the repulsion of the polar head groups opposes self-assembly [11, 12]. In addition, the atoms in functional groups, like the amide bond found in amino acid-based surfactants, often form intermolecular hydrogen bonds that in turn play an important role in determining the size and shape of surfactant micelles [11–13].

Amino acid-based surfactants have become increasingly popular in recent years because they are environmentally benign, abundant, and quite versatile [11–19]. Surfactants with amino acid head groups have both amide and carboxylic acid functional groups; therefore, solution pH would be expected to affect the percentage ionization of the carboxylate groups and the rate at which amide protons exchange with solvent [19–21]. The degree of head group ionization and the amide proton solvent exchange rate would in turn be expected to affect micelle physical properties like CMC, size, and aggregation number [12, 22].

This study investigated the effect of solution pH on the physical properties of micelles formed by the amino acidbased surfactant undecylenyl L-leucine (und-Leu). The surfactant's structure is shown in Fig. 1c. Fluorescence experiments with the fluorophore pyrene were used to measure the surfactant's CMC and micelle aggregation numbers as a function of solution pH [23]. Nuclear magnetic resonance (NMR) spectroscopy was used to measure the diffusion coefficients (D) of the micellar aggregates [24–28]. The Stokes–Einstein equation was then used to calculate micelle hydrodynamic radii from these D values. NMR-derived micelle radii were compared to radii measured using dynamic light scattering (DLS). Viscosity

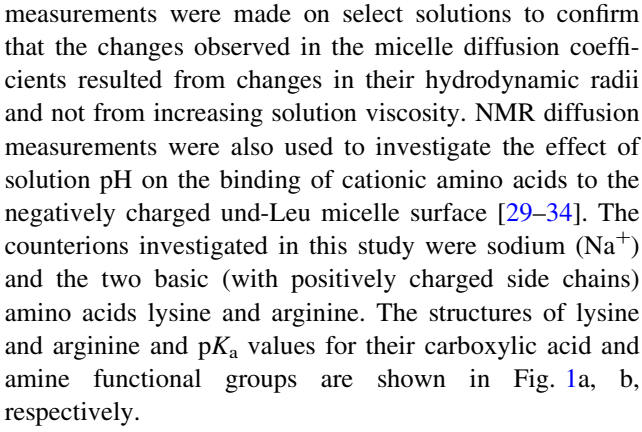
(a)

pKa = 10.5+H₃N

(c)

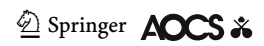
Fig. 1 Chemical structures and pK_a values for a L-lysine and **b** L-arginine. **c** Chemical structure of L-undecyl leucinate

Experimental Procedures All reagents used to prepare the surfactant solutions were **(b)** pKa = 2.2pKa = 12.5pKa = 2.2 NH_2 NH₃ NH_3 + pKa = 9.0pKa = 9.0



Finally, as with all amino acid-containing compounds, the amide moieties in the und-Leu surfactant molecules are capable of forming inter- and intramolecular hydrogen bonds. H-bonding among the polar head groups may play a role in determining their conformation. In addition, it is well known that amide protons in peptides and proteins undergo both acid- and base-catalyzed exchange with solvent protons in aqueous solutions [21]. NMR spectroscopy was, therefore, used to measure the rate constants for the base-catalyzed und-L-Leu amide proton/solvent exchange reaction. The effect of micelle formation on the magnitude of these rate constants was then investigated.

purchased from Sigma Aldrich. Solutions containing the surfactant and equimolar concentrations of NaHCO3 (99.5 %), L-lysine (>98 %), D-lysine (>98 %), L-arginine (≥98 %), or D-arginine (≥98 %) were prepared gravimetrically in a solvent containing 90 % deionized water and 10 % deuterium oxide (99.9 % atom). Surfactant solutions



were passed through a 0.2- μ m syringe filter and were allowed to equilibrate at 25 °C before experiments were performed.

Basic pH adjustments were made by adding solid sodium hydroxide (97 %) or a concentrated NaOH_(aq) solution to the surfactant solutions. Acidic pH adjustments were made by the addition of concentrated deuterium chloride. Microliter additions of acid or base were made to minimally affect the total volume of solution. A three-point calibration was done with the pH meter before measurements were made. In each diffusion experiment performed above the CMC, a small volume of tetramethylsilane (≥99.9 %) (TMS) was added to each NMR tube. The solutions were then mixed and allowed to equilibrate to allow the TMS to solubilize in the micelle core [24].

Surfactant Synthesis

Surfactant monomers were prepared by mixing the *N*-hydroxysuccinimide ester of undecylenic acid with L-leucine to form *N*-undecylenyl L-leucinate surfactant [35]. The purity of the surfactants was confirmed with proton NMR and high-performance liquid chromatography (HPLC).

Dynamic Light Scattering Measurements

Dynamic light scattering (DLS) measurements were performed using a Malvern Nano Series Zetasizer at a scattering angle of 173° . All solvents used for DLS measurements were passed through a $0.020\text{-}\mu\text{m}$ filter and pHs of the surfactant solutions were adjusted as described above. After preparation, surfactant solutions were filtered again using a $0.20\text{-}\mu\text{m}$ filter before DLS measurements were made.

Critical Micelle Concentration Measurements

Fluorescence measurements were performed using a SPEX model F2T211 spectrofluorometer equipped with a thermostated cell housing and a thermoelectrically cooled Hamamatsu R928 photomultiplier tube. All measurements were made at 25 °C. To determine the CMC, 50 mM surfactant and 1×10^{-7} mM pyrene solutions were prepared. The pH of each solution was adjusted as needed with either HCl_(aq) or NaOH_(aq). The solutions were then diluted, keeping the concentration of pyrene constant. Excitation was carried out at 337 nm and emission intensities were measured at 372 nm and 385 nm. A plot of the pyrene I/III ratio vs. surfactant concentration was used to determine the CMC. Pyrene is a commonly used fluorescent probe for determination of CMC [36]. Pyrene has significant fine structure in its emission spectrum, with five vibronic bands

at 372, 379, 385, 388, and 393 nm. The first vibronic band at 372 nm is relatively insensitive to the compound's environment, whereas the third vibronic band at 385 nm is much more sensitive. Thus, a ratio of the intensities of the two peaks can be used to measure changes in the pyrene molecule's microenvironment. This ratio changes significantly as micelles begin to form and pyrene moves from the aqueous phase into the more hydrophobic environment within the micellar core [36].

Aggregation Number Measurements

Solutions similar to those used in the CMC studies were prepared to measure und-Leu micelle aggregation numbers. The solutions used in the aggregation number measurements, though, also contained increasing concentrations of the fluorescence quencher (N-acetylpyridinum chloride). The intensities of the pyrene fluorescence, I, in solutions containing a quencher concentration [Q] were measured along with the pyrene fluorescence intensity in solutions with no quencher, I_0 . Equation 1 relates these values to the micelle aggregation number, N, and the surfactant CMC [23]. C_s is the total surfactant concentration.

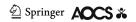
$$\ln\left(\frac{I_{o}}{I}\right) = \frac{N \times [Q]}{C_{s} - \text{CMC}} \tag{1}$$

The aggregation number, N, was calculated from the slope of a plot of $ln(I_0/I)$ vs [Q] [23].

NMR Diffusion Experiments

NMR diffusion coefficient measurements were done at 25.0 °C on a Bruker 400 MHz spectrometer. The spectrometer's probe contained an actively shielded z-gradient coil that produced a maximum gradient strength of 40.0 G cm⁻¹. The bipolar pulse pair encode-decode pulse sequence was used for the diffusion coefficient measurements [37]. In each diffusion experiment, 20 NMR spectra were collected with magnetic field gradient strengths ranging from 2.5 to 30.2 G cm⁻¹. At each gradient value, the gradient pulse duration, δ , was 4.0 ms, the short delay between the bipolar gradients, τ , was 0.20 ms, and the diffusion time, Δ , was 250.0 ms. The H₂O peak in each spectrum was removed by incorporating the WATER-GATE water suppression method into the diffusion pulse sequence [38]. The spectral width in all NMR spectra was 6173 Hz. Three replicate trials were performed on each sample.

After data collection, each FID was apodized with 1.0 Hz line broadening, Fourier transformed, and baseline corrected. Relative to TMS, the resonances used in the diffusion coefficient measurements were 3.3 and 3.8 ppm for arginine, 3.1 and 3.8 ppm for lysine, and the



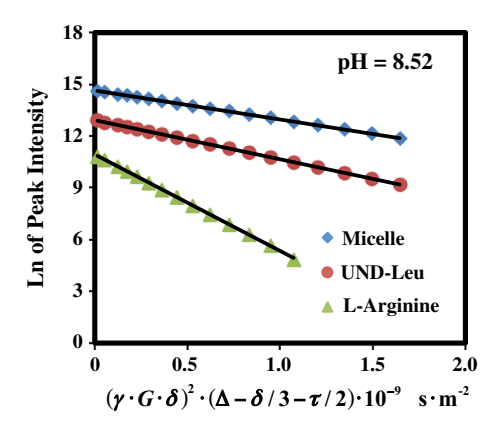


Fig. 2 Representative plot of NMR peak intensity versus the quantity $(\gamma G \delta)^2 (\Delta - \delta/3 - \tau/2)$ for a solution containing 50.0 mM und-Leu, 50 mM L-Arginine, and TMS at pH 8.52. The slope of each line equals -D

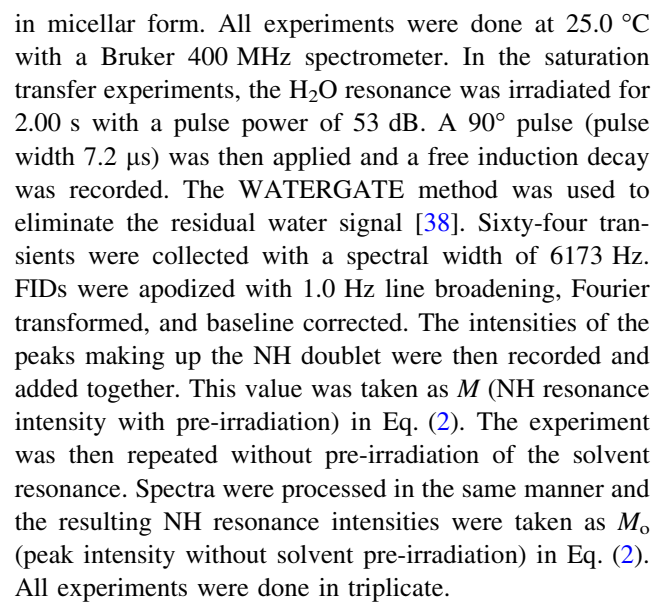
surfactant's methylene chain resonance at 1.3 ppm. The intensities of these peaks were recorded at each gradient strength. Plots were prepared of the natural log of the peak intensity versus the quantity $(\gamma G \delta)^2 (\Delta - \delta/3 - \tau/2)$ where γ is the magnetogyric ratio, δ is the magnetic field gradient duration, τ is the short delay between the bipolar gradients, and Δ is the diffusion time [24, 37]. A linear regression analysis was used to calculate the slope of the resulting lines, which was in turn were taken as -D, where D is the arginine, lysine, or the surfactant diffusion coefficient. The R^2 values for all linear fits were greater than 0.99. A representative NMR diffusion plot is shown in Fig. 2.

ROESY NMR

Phase-sensitive ROESY spectra were acquired by co-adding 400 transients measured into 2048 F2 data points for each of 256 increments in F1. A linear prediction analysis was used to extend the data set in F1 by 200 points. Zero filling was then done to generate a 2048 \times 1024 point data set. A π /2-shifted sine bell squared apodization function was applied in F1 and F2, and then the data set was Fourier transformed and phased in both dimensions. The ROESY spin lock time was 200 ms.

Saturation Transfer

NH–solvent exchange rate constants, $k_{\rm ex}$, were measured with the saturation transfer method developed by Forsen and Hoffman [39]. Solutions containing either 10.0 or 50.0 mM surfactant were prepared by the methods described above. The former concentration allowed $k_{\rm ex}$ to be measured for the surfactant monomers and the latter concentration provided for measurements with the surfactants



The standard inversion-recovery experiment was used to measure the spin lattice relaxation time, T1, for the surfactant's NH resonance at pH 7.5. These experiments provided a T1 value in the absence of NH proton exchange. In the inversion-recovery experiments, 15 spectra were collected with 64 transients and a spectral width of 6173 Hz. The experiment's τ values were incremented from 1.0 ms to 2.0 s. T1 measurements were made in triplicate.

The NH-solvent exchange rate constant was calculated from the M, M_0 , and T1 values using Eq. (2) [40].

$$\left(\frac{M}{M_{\rm o}}\right) = \frac{1}{1 + k_{\rm ex} \times T1} \tag{2}$$

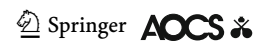
Liner plots were then prepared of the $k_{\rm ex}$ values versus $[{\rm OH^-}]$. The slope of these lines was taken as the base-catalyzed amide proton solvent exchange rate constant, $k_{\rm OH}$. This analysis is described in more detail below.

Viscosity Measurements

Viscosity measurements were made with a glass capillary Ostwald viscometer. Because this method provides relative viscosity measurements, a liquid of known viscosity (deionized water) was used as a reference. The relative viscosity (η_r) of the surfactant solutions was calculated with Eq. (3), where t and t_0 are the measured times in seconds of the surfactant solution and the reference liquid, respectively, and ρ and ρ_0 are their respective densities.

$$\eta_{\rm R} = \frac{t}{t_0} \times \frac{\rho}{\rho_0} \tag{3}$$

The absolute viscosity of each surfactant solution was calculated with Eq. (4), where η is the absolute viscosity of



the solution and η_0 is the absolute viscosity of the reference liquid.

$$\eta_{\rm R} = \frac{\eta}{\eta_{\rm o}} \tag{4}$$

The time for deionized water (the reference liquid) to travel through the viscometer was measured in triplicate with a stopwatch and then averaged to provide the value t_0 . The surfactant solution was timed in the same manner to provide a value for t in Eq. (3) at each pH. During all measurements, the viscometer was submerged in a water bath at 25.0 °C. Before viscosity measurements were made, all solutions were equilibrated in the water bath. The literature density of water at 25.0 °C (0.99701 g mL⁻¹) was used for ρ_0 , while the literature water viscosity at 25.0 °C (0.8904 cP) was used for η_o [41]. The density of the surfactant solutions was measured at each pH by weighing 1.00-mL aliquots.

Results and Discussion

The results of the surfactant solution viscosity measurements as a function of pH are shown in Table 1. For each surfactant solution, very little change in the viscosity was observed when moving from slightly acidic to basic pH. There are also no trends evident in the data that suggest the surfactant solutions become consistently more or less viscous at either high or low pH in the presence of Na⁺, arginine, or lysine counterions. Therefore, it can be concluded that changing the pH of the und-Leu solutions did not affect the solutions' viscosities in a significant way and that changes in the micelle diffusion coefficients observed in the NMR experiments likely do not result from changes in solution viscosity as a function of pH.

Micelle Radii Measurements

NMR diffusion experiments were performed with 50 mM und-Leu surfactant solutions. Each solution was spiked

with a small quantity of tetramethylsilane, TMS. The TMS solubilized inside the micelle core and thus reported the diffusion coefficient of the micelle [24]. The micelle diffusion coefficient, calculated from the decay in the intensity of the TMS resonance with increasing gradient strength, was smaller than the diffusion coefficient measured by monitoring the decay of the surfactant resonances. This effect was observed because during the diffusion measurements, the surfactant molecules underwent fast exchange between the micelles and free solution [24]. Therefore, the diffusion coefficient measured for the surfactants (D_{obs}) was the weighted average of the slower micelle-bound (D_{micelle}) and faster free solution (D_{free}) values. Given this relationship, Eq. (5) was used to calculate the fraction of the surfactant monomers bound to the micelles, represented by $f_{b,surf}$, at each pH

$$D_{\text{obs}} = f_{\text{b.surf}} \times D_{\text{micelle}} + (1 - f_{\text{b.surf}}) \times D_{\text{free}}$$
 (5)

The und-Leu free solution diffusion coefficient ($D_{\rm free}$) was (6.04 \pm 0.04) \times 10⁻¹⁰ m² s⁻¹. $D_{\rm free}$ was measured by carrying out diffusion experiments on a 10.0 mM solution of the und-L-Leu surfactant. This concentration was below the surfactant's CMC; therefore, the und-Leu surfactant was in monomeric form.

The micelle diffusion coefficients ($D_{\rm micelle}$) were also used to calculate the hydrodynamic radii of the micelles at each pH investigated. Hydrodynamic radius is defined as the radius of the sphere with the same diffusion coefficient as the micelle [42]. Radius calculations were done with the Stokes–Einstein equation (Eq. (6)) where $D_{\rm micelle}$ is the micelle diffusion coefficient, $k_{\rm B}$ is Boltzmann's constant, T is absolute temperature, η is the viscosity, and $R_{\rm h}$ is the micelle hydrodynamic radius.

$$D_{\text{micelle}} = \frac{k_{\text{B}} \times T}{6 \times \pi \times \eta \times R_{\text{h}}} \tag{6}$$

 $D_{
m micelle}$, $D_{
m obs}$, $f_{
m b,surf}$, and $R_{
m h}$ values for the und-Leu surfactant solutions containing ${
m Na}^+_{
m (aq)}$ counterions are given in Table 2.

Table 1 Surfactant solution viscosities as a function of pH for solutions containing 50 mM und-Leu and 50 mM NaHCO₃ (Na⁺ counterions), 50 mM und-Leu and 50 mM L-arginine, and 50 mM und-Leu and 50 mM L-lysine

50 mM und-Leu and 50 mM NaHCO ₃		50 mM und-l	Leu and 50 mM L-Arginine	50 mM und-Leu and 50 mM L-lysine		
pH	Viscosity (cP)	pН	Viscosity (cP)	pH	Viscosity (cP)	
6.69	1.04 ± 0.02	6.50	1.00 ± 0.03	6.51	1.03 ± 0.01	
7.61	1.06 ± 0.06	7.50	1.01 ± 0.01	7.51	1.02 ± 0.03	
8.54	1.03 ± 0.03	8.50	1.04 ± 0.03	8.53	1.01 ± 0.02	
9.57	1.05 ± 0.01	9.50	1.03 ± 0.02	9.42	1.01 ± 0.04	
10.67	1.03 ± 0.02	10.50	1.00 ± 0.02	10.62	0.97 ± 0.01	
11.62	1.05 ± 0.02	11.50	1.05 ± 0.01	11.53	0.99 ± 0.03	

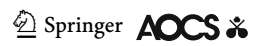


Table 2 Diffusion coefficients, fraction bound (f_b) values, hydrodynamic radii, critical micelle concentrations (CMC), and micelle aggregation numbers versus pH for solutions containing 50 mM und-Leu and 50 mM NaHCO₃

pН	$D_{\rm obs} \times 10^{10}$ UND-Leu (m ² s ⁻¹)	$D_{\text{mic}} \times 10^{10}$ $(\text{m}^2\text{s}^{-1})$	$f_{ m b}$ UND-Leu	$R_{\rm h}$ (Å) (NMR)	$R_{\rm h}$ (Å) (DLS)	CMC (mM)	$N_{ m agg}$
7.5	2.87 ± 0.01	2.29 ± 0.01	0.844 ± 0.006	9.4 ± 0.2	10.9 ± 0.5	17 ± 1	60 ± 5
8.0	2.83 ± 0.04	2.35 ± 0.01	0.870 ± 0.008	9.2 ± 0.1	10.9 ± 0.5	19 ± 1	61 ± 5
8.5	2.88 ± 0.01	2.35 ± 0.01	0.855 ± 0.006	9.2 ± 0.1	10.3 ± 0.5	19 ± 1	60 ± 5
9.0	2.86 ± 0.02	2.27 ± 0.01	0.843 ± 0.006	9.5 ± 0.1	10.2 ± 0.5	19 ± 1	58 ± 5
9.5	2.92 ± 0.01	2.35 ± 0.01	0.847 ± 0.005	9.2 ± 0.1	10.8 ± 0.5	19 ± 1	59 ± 5
10.0	2.82 ± 0.01	2.31 ± 0.02	0.863 ± 0.006	9.3 ± 0.1	11.3 ± 0.5	19 ± 1	60 ± 5
10.5	2.76 ± 0.01	2.02 ± 0.01	0.815 ± 0.006	10.7 ± 0.1	11.4 ± 0.5	19 ± 1	50 ± 5
11.0	2.81 ± 0.01	2.15 ± 0.04	0.830 ± 0.006	10.0 ± 0.2	11.5 ± 0.5	20 ± 1	45 ± 5
11.5	2.81 ± 0.01	2.16 ± 0.04	0.836 ± 0.006	10.0 ± 0.2	11.5 ± 0.5	21 ± 1	47 ± 5

Table 3 Diffusion coefficients, fraction bound (f_b) values, hydrodynamic radii, critical micelle concentrations (CMC), and micelle aggregation numbers versus pH for solutions containing 50 mM und-Leu and 50 mM L-arginine

pН	$D_{\rm obs} \times 10^{10}$ UND-Leu (m ² s ⁻¹)	$D_{\rm obs} \times 10^{10}$ Arginine $({\rm m}^2 {\rm s}^{-1})$	$D_{\text{mic}} \times 10^{10}$ (m ² s ⁻¹)	f _b UND-Leu	f _b Arginine	R _h (Å) (NMR)	CMC (mM)	$N_{ m agg}$
7.5	2.20 ± 0.01	5.63 ± 0.03	1.44 ± 0.01	0.879 ± 0.006	0.38 ± 0.02	14.3 ± 0.1	14 ± 1	104 ± 5
8.0	2.25 ± 0.01	5.64 ± 0.01	1.40 ± 0.01	0.856 ± 0.007	0.38 ± 0.02	14.7 ± 0.1	15 ± 1	105 ± 5
8.5	2.28 ± 0.01	5.59 ± 0.03	1.44 ± 0.01	0.862 ± 0.006	0.39 ± 0.01	14.3 ± 0.1	15 ± 1	98 ± 5
9.0	2.29 ± 0.01	5.58 ± 0.01	1.58 ± 0.01	0.841 ± 0.006	0.39 ± 0.01	13.0 ± 0.1	15 ± 1	100 ± 5
9.5	2.17 ± 0.01	6.28 ± 0.03	1.65 ± 0.01	0.881 ± 0.006	0.28 ± 0.01	12.5 ± 0.1	16 ± 1	93 ± 5
10.0	2.32 ± 0.01	6.97 ± 0.05	1.84 ± 0.01	0.886 ± 0.006	0.18 ± 0.01	11.2 ± 0.1	16 ± 1	104 ± 5
10.5	2.26 ± 0.01	7.22 ± 0.02	1.96 ± 0.02	0.926 ± 0.007	0.14 ± 0.01	10.5 ± 0.1	18 ± 1	94 ± 5
11.0	2.56 ± 0.01	7.44 ± 0.08	2.05 ± 0.02	0.872 ± 0.006	0.11 ± 0.02	10.0 ± 0.1	22 ± 1	95 ± 5
11.5	2.53 ± 0.01	7.50 ± 0.06	2.00 ± 0.02	0.868 ± 0.007	0.10 ± 0.01	10.3 ± 0.1	22 ± 1	95 ± 5

To study the effect of counterion binding on the physical properties of the und-Leu micelles, NMR diffusion experiments were performed as a function of pH with solutions containing 50 mM und-Leu and 50 mM of either the L- or D-form of arginine (Arg) or lysine (Lys). Data for the L-amino acid studies are shown in Tables 3 and 4. Results from the D-amino acid measurements are shown in Tables 5 and 6. As shown in Fig. 1a and b, the pK_a of the primary amine for both amino acids is approximately 9.0 [43]. Thus, lysine and arginine are cationic (effective positive charge) below pH 9.0 and zwitterionic above pH 9.0. As a result, arginine and lysine would both be expected to have a much stronger electrostatic attraction to the negatively charged micelles in their cationic form below pH 9.0 [43].

NMR-derived diffusion coefficients for und-Leu, with lysine and arginine counterions and solubilized TMS molecules were measured as described above. These diffusion coefficients were then used to calculate the fraction of both surfactant monomers and arginine or lysine

molecules associated with the micelles as a function of pH. Micelle radii were also calculated for solutions containing the surfactant micelles and $\mathrm{Na}_{(\mathrm{aq})}^+$, lysine or arginine counterions. In the presence of the anionic micelles, cationic lysine or arginine molecules experience fast exchange on the NMR time scale between free solution and micelle-bound states [29]. Therefore, as with the surfactant monomers, the observed diffusion coefficient of lysine or arginine ($D_{\mathrm{obs,lys}}$ or $D_{\mathrm{obs,arg}}$) is the weighted average of the free solution and micelle-bound values. This behavior is shown in Eq. (7) for arginine. An analogous equation holds for lysine. In Eq. (7), $f_{\mathrm{b,arg}}$ is the mole fraction of arginine molecules bound to the micelle, D_{micelle} is the micelle diffusion coefficient, and $D_{\mathrm{free,arg}}$ is the arginine diffusion coefficient in free solution [24, 29].

$$D_{\text{obs,arg}} = f_{\text{b,arg}} \times D_{\text{micelle}} + (1 - f_{\text{b,arg}}) \times D_{\text{free}}$$
 (7)

 $D_{\rm free}$ values for lysine and arginine were (7.08 \pm 0.06) \times 10⁻¹⁰ m² s⁻¹ and (6.73 \pm 0.01) \times 10⁻¹⁰ m² s⁻¹, respectively.

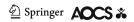


Table 4 Diffusion coefficients, fraction bound (f_b) values, hydrodynamic radii, critical micelle concentrations (CMC), and micelle aggregation numbers versus pH for solutions containing 50 mM und-Leu and 50 mM L-lysine

pН	$D_{\rm obs} \times 10^{10}$ UND-Leu (m ² s ⁻¹)	$D_{\rm obs} \times 10^{10}$ Lysine (m ² s ⁻¹)	$D_{\text{mic}} \times 10^{10}$ (m ² s ⁻¹)	$f_{ m b}$ UND-Leu	f _b Lysine	R _h (Å) (NMR)	CMC (mM)	$N_{ m agg}$
7.50	2.13 ± 0.01	5.69 ± 0.01	1.59 ± 0.01	0.879 ± 0.007	0.37 ± 0.01	12.8 ± 0.1	18 ± 1	82 ± 5
8.0	2.25 ± 0.01	5.76 ± 0.01	1.66 ± 0.01	0.865 ± 0.006	0.36 ± 0.01	12.3 ± 0.1	19 ± 1	71 ± 5
8.5	2.27 ± 0.01	5.85 ± 0.06	1.72 ± 0.01	0.870 ± 0.006	0.35 ± 0.01	12.0 ± 0.1	19 ± 1	85 ± 5
9.0	2.29 ± 0.01	6.06 ± 0.04	1.71 ± 0.01	0.866 ± 0.007	0.32 ± 0.01	12.0 ± 0.1	19 ± 1	86 ± 5
9.5	2.31 ± 0.01	6.77 ± 0.06	1.84 ± 0.01	0.887 ± 0.006	0.21 ± 0.01	11.2 ± 0.1	19 ± 1	89 ± 5
10.0	2.31 ± 0.01	7.06 ± 0.02	1.80 ± 0.01	0.879 ± 0.007	0.17 ± 0.01	11.4 ± 0.1	20 ± 1	95 ± 5
10.5	2.26 ± 0.01	7.49 ± 0.02	1.74 ± 0.01	0.878 ± 0.007	0.10 ± 0.03	11.8 ± 0.1	20 ± 1	98 ± 5
11.0	2.18 ± 0.02	7.93 ± 0.09	1.72 ± 0.01	0.892 ± 0.008	0.03 ± 0.02	12.0 ± 0.1	22 ± 1	105 ± 5
11.50	2.01 ± 0.01	7.98 ± 0.03	1.64 ± 0.01	0.922 ± 0.008	0.02 ± 0.01	12.3 ± 0.1	23 ± 1	110 ± 5

Table 5 Diffusion coefficients, fraction bound (f_b) values, hydrodynamic radii, critical micelle concentrations, and micelle aggregation numbers versus pH for solutions containing 50 mM und-Leu and 50 mM p-arginine

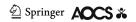
рН	$D_{\text{obs}} \times 10^{10}$ UND-Leu (m ² s ⁻¹)	$D_{\rm obs} \times 10^{10} \text{Arginine}$ $(\text{m}^2 \text{s}^{-1})$	$D_{\text{mic}} \times 10^{10}$ (m ² s ⁻¹)	f _b UND-Leu	f _b D-Arginine	$R_{\rm h}$ (Å) (NMR)
7.5	1.94 ± 0.01	5.33 ± 0.02	1.39 ± 0.01	0.882 ± 0.007	0.41 ± 0.02	14.6 ± 0.1
8.0	1.96 ± 0.01	5.32 ± 0.01	1.41 ± 0.01	0.880 ± 0.007	0.42 ± 0.01	14.7 ± 0.1
8.5	2.00 ± 0.01	5.32 ± 0.02	1.42 ± 0.01	0.874 ± 0.006	0.42 ± 0.01	14.5 ± 0.1
9.0	2.08 ± 0.01	5.39 ± 0.03	1.43 ± 0.01	0.858 ± 0.006	0.41 ± 0.01	14.4 ± 0.1
9.5	2.21 ± 0.01	6.03 ± 0.03	1.61 ± 0.01	0.865 ± 0.007	0.32 ± 0.01	12.8 ± 0.1
10.0	2.39 ± 0.01	6.61 ± 0.07	1.81 ± 0.01	0.863 ± 0.007	0.24 ± 0.01	11.4 ± 0.1
10.5	2.32 ± 0.01	7.18 ± 0.01	1.80 ± 0.01	0.876 ± 0.007	0.15 ± 0.01	11.5 ± 0.1
11.0	2.44 ± 0.04	7.28 ± 0.06	1.96 ± 0.01	0.883 ± 0.009	0.14 ± 0.01	10.5 ± 0.3
11.5	2.61 ± 0.01	7.62 ± 0.05	2.18 ± 0.02	0.888 ± 0.006	0.08 ± 0.01	9.4 ± 0.1

Table 6 Diffusion coefficients, fraction bound (f_b) values, hydrodynamic radii, critical micelle concentrations, and micelle aggregation numbers versus pH for solutions containing 50 mM und-Leu and 50 mM p-lysine

рН	$D_{\rm obs} \times 10^{10} \text{ UND-Leu } (\text{m}^2 \text{s}^{-1})$	$D_{\rm obs} \times 10^{10}$ D-Lysine (m ² s ⁻¹)	$D_{\rm mic} \times 10^{10} (\rm m^2 s^{-1})$	f _b UND-Leu	f _b D-Lysine	R _h (Å) (NMR)
7.5	2.16 ± 0.06	5.92 ± 0.09	2.08 ± 0.02	0.845 ± 0.010	0.36 ± 0.02	9.9 ± 0.1
8.0	2.19 ± 0.07	5.97 ± 0.05	2.04 ± 0.01	0.851 ± 0.011	0.35 ± 0.03	10.1 ± 0.1
8.5	2.27 ± 0.07	5.91 ± 0.08	2.10 ± 0.01	0.839 ± 0.012	0.37 ± 0.02	9.8 ± 0.1
9.0	2.77 ± 0.01	6.44 ± 0.06	2.08 ± 0.01	0.826 ± 0.004	0.28 ± 0.01	9.9 ± 0.1
9.5	2.74 ± 0.01	6.90 ± 0.05	2.17 ± 0.01	0.852 ± 0.004	0.20 ± 0.01	9.5 ± 0.1
10.0	2.74 ± 0.01	7.29 ± 0.09	2.12 ± 0.01	0.843 ± 0.005	0.14 ± 0.02	9.7 ± 0.1
10.5	2.74 ± 0.01	7.67 ± 0.07	2.18 ± 0.02	0.854 ± 0.005	0.07 ± 0.01	9.5 ± 0.1
11.0	2.63 ± 0.02	7.79 ± 0.01	2.07 ± 0.01	0.859 ± 0.005	0.05 ± 0.01	10.0 ± 0.1
11.5	2.43 ± 0.01	7.80 ± 0.06	1.85 ± 0.01	0.862 ± 0.005	0.05 ± 0.01	11.2 ± 0.1

Und-Leu Solutions with $Na_{(aq)}^{+}$ Counterions

The first step in analyzing counterion binding to the und-Leu micelles was to determine the fraction of surfactant molecules in the micellar form ($f_{b,surf}$). Table 2 shows that over the entire pH range, when sodium was used as the counterion, $f_{\rm b,surf}$ values for und-Leu were between ca. 0.82 and 0.87, indicating that on average at least ca. 82 % of surfactant monomers were bound to micellar aggregates at each pH investigated. Table 2 also



shows that when sodium was used as the counterion, the pH of the solution had only a modest effect on the hydrodynamic radii of the micelles. Micelle radii were found to range from ca. 9.2 to 10.7 Å, with the larger radii occurring at higher pH. One possible explanation for the slightly larger radii at higher pH could be due to a decrease in hydrogen bonding between the amino acid polar head groups owing to faster exchange of the NH proton with $\rm H_2O$. This decrease in hydrogen bonding would be expected to increase the spacing between the polar head groups, allowing more water to penetrate into the micellar head group region and thus causing the micelle to swell.

The effect of pH on the und-Leu micelle hydrodynamic radii in solutions with $Na^+_{(aq)}$ counterions was also investigated using DLS. Figure 3 compares the hydrodynamic radii measured using DLS with the radii from NMR. There is very good agreement between the two techniques, with each showing that und-Leu formed relatively small micelles with radii in the 10~Å range and that micelle size in the $Na^+_{(aq)}$ -containing solutions did not change appreciably or in any systematic manner with increasing solution pH.

Table 2 also shows how the und-Leu surfactant CMC changed as a function of solution pH. The CMC of und-Leu with sodium as the counterion ranged from 17 at pH 7.5 to 21 at pH 11.5. Similar to the hydrodynamic radius, pH does not appear to have a significant effect on the surfactant's CMC. However, a slight decrease in aggregation number of the und-Leu micelles was observed with increasing pH. The aggregation number of und-Leu was about 60 at pH 7.5 and then dropped to 47 at pH 11.5. The small decrease in aggregation number could also be related to the proposed looser packing of the monomers within the micelle as a result of a decrease in hydrogen bonding between the und-Leu amino acid polar head groups at high pH.

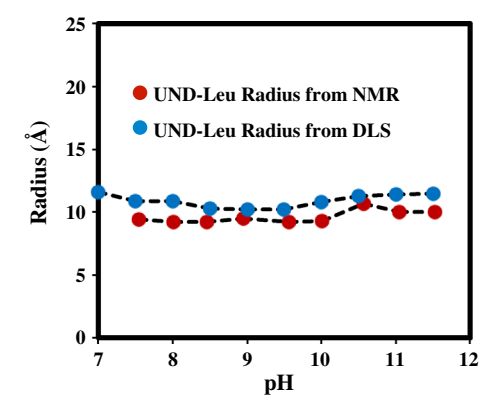


Fig. 3 Comparison of DLS- and NMR-derived micelle hydrodynamic radii versus pH for solutions containing 50.0 mM und-Leu with $\mathrm{Na_{(aq)}^+}$ counterions

Binding of Arginine Counterions

Figure 4a shows plots of $f_{b,arg}$, $f_{b,surf}$, and micelle hydrodynamic radius versus pH for und-Leu micelles with Larginine counterions. The data plotted in Fig. 4a is also shown in Table 3. The $f_{\rm b,arg}$ values from pH 7.5 to 9.0 are all in the 0.39 ± 0.01 range, indicating that at these pHs ca. 39 % of the arginine molecules in the solution are tightly bound to the micelle surface and are diffusing at the same rate as the micellar aggregate. As mentioned previously, at pHs above 9.0 (the pK_a of the arginine's primary amine) arginine starts to become zwitterionic rather than having a net positive charge. At this point the f_{b.arg} values begin to decrease. At pH 9.5 the arginine fraction bound decreases to 0.28 ± 0.01 and by pH 11.5 the $f_{\rm b,arg}$ value is about 10 %. Therefore, the bound arginine molecules begin to dissociate from the micelle once the primary amine deprotonates and dissociation becomes nearly complete at high pH. As arginine dissociates from the micelles, the fraction of surfactant molecules (f_{b. surf}) bound to the micelles remains relatively constant. For example, with und-Leu at pH 7.5 to 9.0 when the $f_{b,arg}$ value is at its maximum, $f_{b,surf}$ averages 0.86 ± 0.01 . At pH 9.5 when the arginine begins to dissociate from the micelle, $f_{\rm b,surf}$ is 0.87 \pm 0.01. At pH 11.5 when the arginine is fully dissociated, $f_{b,surf}$ is 0.87 ± 0.01 . These $f_{b,surf}$ values are also marginally larger than those measured in solutions containing Na_(a0)⁺ counterions (Table 2).

While the fraction of bound surfactant molecules remains constant as a function of pH in the L-argininecontaining und-Leu solutions, the micelle radius does not. At pH 8.0 the micelle diffusion coefficient is $(1.40 \pm 0.01) \times 10^{-10} \,\mathrm{m}^2 \,\mathrm{s}^{-1}$, corresponding to a hydrodynamic radius of 14.6 \pm 0.1 Å. Note that this R_h value is larger than the 9.2 \pm 0.1 Å radius measured at this pH in the solution with sodium counterions (Table 2). From pH 10.0 to 11.5, the radius decreases from 11.2 ± 0.1 to 10.3 ± 0.1 Å, respectively. The steady decrease in micelle radius mirrors the decrease in fraction of bound arginine molecules shown in Fig. 4a. At pH 11.5, the und-Leu radius in the arginine-containing solutions is similar to the radius of 10.0 ± 0.2 Å measured with sodium counterions (Table 2). The hydrodynamic radius measured in the diffusion experiments corresponds to the radius of the diffusing micelle in solution, including all of its bound counterions [29]. Therefore, the und-Leu micelles are likely larger when arginine is bound simply because of the presence of the arginine molecules at the micelle surface. Then when pH is increased and the L-arginine counterions dissociate from the micelle surface, the und-Leu micelle radius decreases.

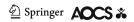
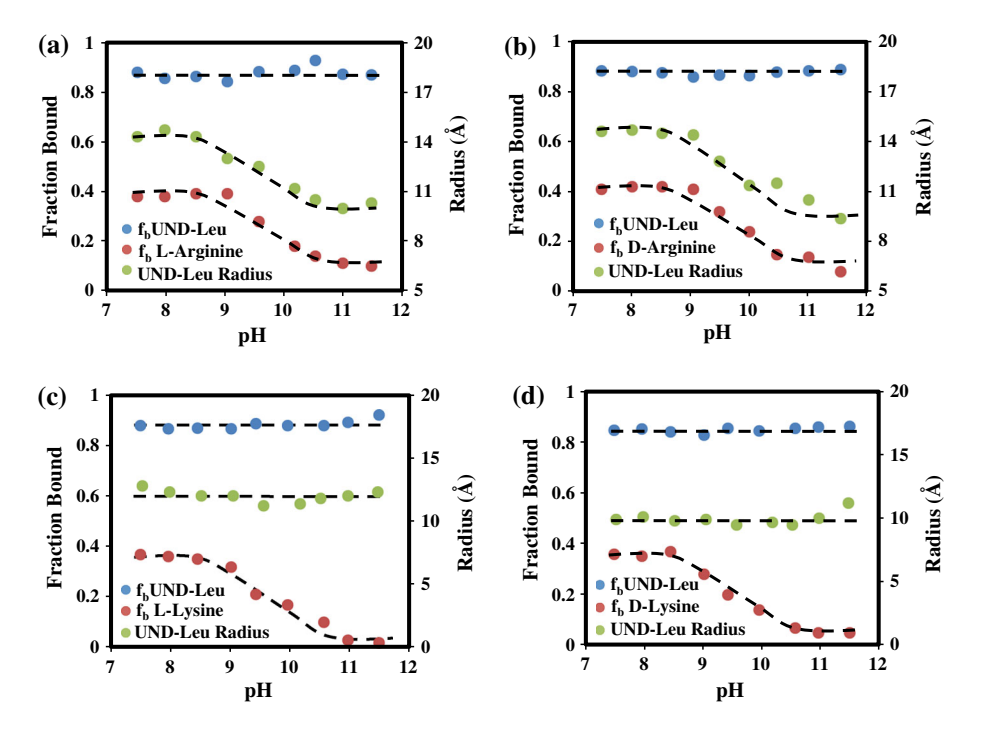


Fig. 4 f_{b,surf}, f_{b,arg}, f_{b,lys}, and und-Leu micelle hydrodynamic radii for solutions containing a 50 mM und-Leu and 50 mM L-arginine, b 50 mM und-Leu and 50 mM D-arginine, c 50 mM und-Leu and 50 mM L-lysine, and d 50 mM und-Leu and 50 mM D-lysine



In order to gain further insight into the structure of the und-Leu micelles with L-arginine counterions, a two-dimensional rotating frame Overhauser enhancement spectroscopy (ROESY) spectrum was collected for a 50 mM Larginine and 50 mM und-Leu mixture at pH 8.0. Diffusion measurements discussed above show that L-arginine is bound to the micelle at this pH. In the ROESY spectrum, there was significant overlap between the L-arginine and und-Leu resonances. However, from 3.0 to 4.2 ppm, the Larginine Hδ, L-arginine Hα, and und-Leu Hα resonances were well resolved as were the und-Leu H δ head group methyl resonances at 0.80 ppm. A portion of the ROESY spectrum containing well-resolved cross peaks between und-Leu and L-arginine resonances is shown in Fig. 5a. ROESY is a 2D-NMR technique where cross peaks are observed when protons that are within ca. 5 Å [44]. ROESY was used for this study because it is less sensitive than techniques like NOESY to the size and tumbling rate of the molecules in solution. It is, therefore, the preferred method for investigating molecules and intermolecular complexes of intermediate size [44]. Cross peaks in a ROESY spectrum are observed between resonances corresponding to nearby protons in the same molecule. For example, in Fig. 5a, a strong cross peak was observed between the und-Leu H α proton and the und-Leu H δ methyl groups. Intermolecular ROESY cross peaks are observed when association between different molecules brings their protons close to one another. In Fig. 5a, a relatively intense intermolecular cross peak was observed between the L-arginine $H\delta$ protons and the und-Leu $H\delta$

methyl groups, and a weaker intermolecular cross peak was observed between the L-arginine $H\alpha$ proton and the und-Leu $H\delta$ resonances. Overall, the presence of these intermolecular ROESY interactions confirms that the L-arginine cations bind to the micelle surface because ROESY cross peaks are only observed for protons in close spatial proximity.

The L-arginine structure in Fig. 1b shows that the amino acid's H\alpha protons are adjacent to its primary amine group and its $H\delta$ protons are adjacent to the amine group on the amino acid side chain. Therefore, since ROESY cross peaks were observed between und-Leu and both the Larginine $H\alpha$ and $H\delta$ protons, it can be concluded that the amino acid cation interacts with the und-Leu micelles through both of its amine functional groups. However, the ROESY spectrum in Fig. 5a shows that the intermolecular cross peak between the L-arginine Hδ protons and und-Leu is much stronger than the corresponding cross peak between und-Leu and the L-arginine Hα proton. This result is consistent with the L-arginine $H\delta$, and thus the amino acid's side chain amine, spending more time bound to or near the micelle surface than the L-arginine Ha and corresponding primary amine. Therefore, the ROESY spectrum suggests that L-arginine binds to the und-Leu micelles perpendicular to the und-Leu micelle surface primarily through its side chain amine with the rest of the molecule extending into solution. This model is shown in Fig. 6a. If L-arginine associated with the und-Leu micelles in this manner, we would expect the micelle radius when the L-arginine was bound to the micelles to be larger than the



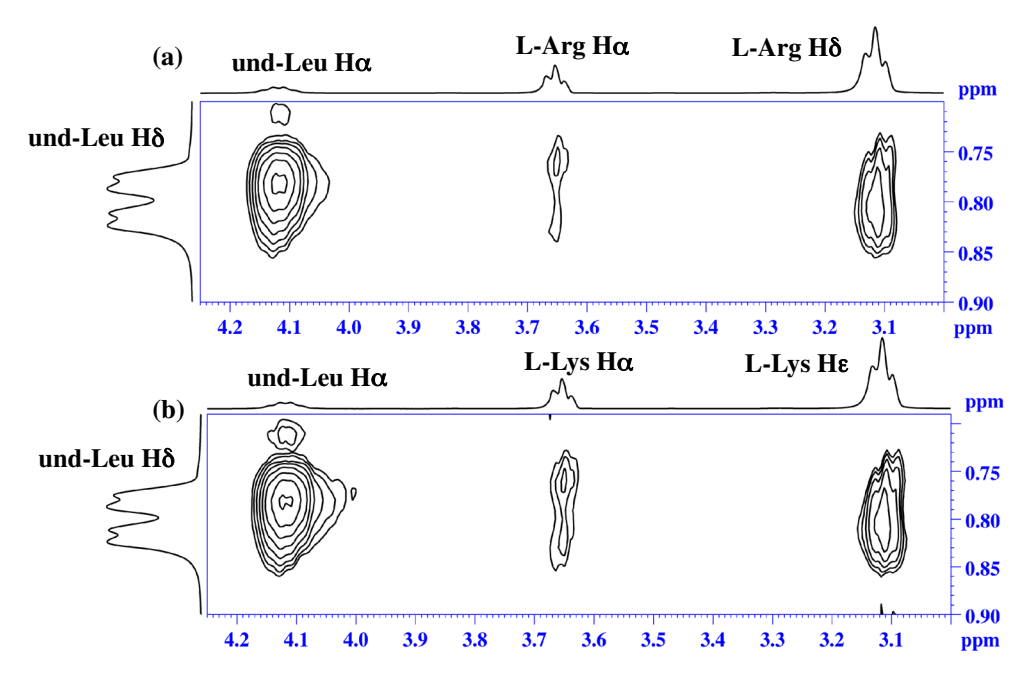


Fig. 5 a A portion of the ROESY spectrum of 50 mM und-Leu and 50 mM L-arginine mixture at pH 8.0. b A portion of the ROESY spectrum of 50 mM und-Leu and 50 mM L-lysine mixture at pH 8.0

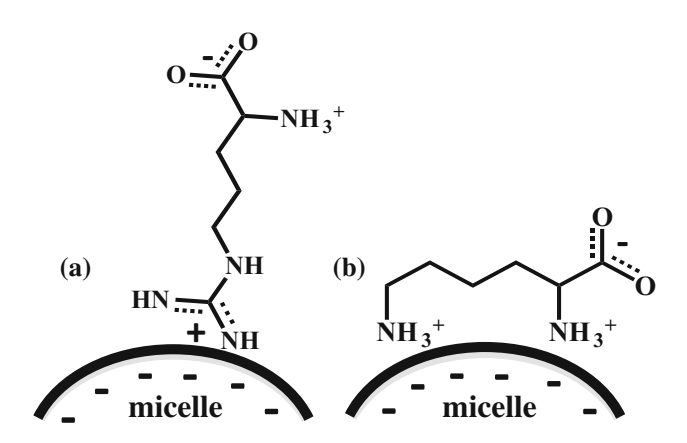


Fig. 6 Model of a L-arginine and b L-lysine binding to und-Leu micelles

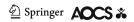
radius of micelles containing $Na_{(aq)}^+$ counterions. The micelle radii measurements in Tables 2 and 3 show this behavior. In addition, if L-arginine bound to the und-Leu micelles in the manner shown in Fig. 6a, when the L-arginine dissociated from the micelle surface at high pH a decrease in the micelle radius would also be expected. Table 3 and Fig. 4a show this behavior as well.

Binding of Lysine Counterions

NMR diffusion experiments were also performed with solutions containing 50 mM und-Leu and equivalent molar concentrations of L-Lysine. The fraction of micelle-bound

lysine and surfactant molecules were calculated along with the micelle hydrodynamic radii in the pH range 7.5–11.5. Table 4 gives $D_{\rm obs,lys}$, $D_{\rm micelle}$, $D_{\rm surfactant}$, $f_{\rm b,lys}$, $f_{\rm b,surf}$, and $R_{\rm h}$ values for each pH investigated along with the CMC and micelle aggregation numbers. The fraction bound and radii data are plotted in Fig. 4c. Measurements with the und-Leu-lysine mixtures show that at pH values less than 9.0, the fraction of bound lysine counterions is less than the corresponding arginine values. For example, at pH 9.0 the $f_{\rm b,arg}$ value is 0.39 ± 0.01 compared to a $f_{\rm b,lys}$ value of 0.32 ± 0.01 at the same pH.

Figure 4c shows other trends in the lysine-containing solutions that are similar to those observed with solutions containing arginine counterions. For example, like arginine at pH 9.0 the primary lysine amine deprotonates and the amino acid becomes a zwitterion rather than having an overall positive charge. Figure 4c shows that at pH 9 the fraction of micelle-bound lysine molecules begins to decrease and becomes almost zero above pH 10. Therefore, like arginine, lysine counterions are only strongly bound to the micelles when they are cationic, but dissociate from the micelles as the primary amine deprotonates. In addition, the $f_{b,surf}$ values plotted in Fig. 4c show that the fraction of surfactant molecules bound to the micelles remains relatively constant as a function of pH. In other words, the fraction of bound surfactant molecules is the same when lysine counterions are bound to the micelles and after they have dissociated at a higher pH values. Finally, as with the arginine-containing solutions, the micelle aggregation numbers in und-Leu solutions containing



counterions are larger than those measured for micelles with $Na^+_{(aq)}$ counterions. The aggregation numbers for the lysine-und-Leu micelles are also comparable to, but marginally smaller than, those of the arginine-und-Leu micelles over the pH range investigated.

Figure 4c, however, shows one interesting difference between the behavior of the micelles in solutions with lysine and arginine counterions. Recall that in the arginine study (Fig. 4a), the micelle hydrodynamic radius decreased as the arginine primary amine deprotonated and the cation dissociated from the micelle. At pH 11.5, the micelle radius in the arginine-containing solutions was comparable to that in solutions containing only Na_(aq) counterions. Figure 4c shows that no such corresponding decrease in micelle radius is observed for the lysine-containing solutions. Instead, moving from pH 7.5 to 11.5, the micelle radii are relatively constant with values ranging from 11.2 to 12.8 Å. Therefore, instead of decreasing when the primary lysine amine deprotonates, the micelle radii remain relatively constant throughout the pH range. In this sense, the behavior of the lysine-containing solutions is more similar to the $Na_{(aq)}^+$ counterion results in Table 2 than the arginine counterion results in Table 3. The different trends observed in the micelle radii versus pH in the arginine- and lysinecontaining solutions suggest that the two amino acid cations associate with the micelles in a slightly different manner.

Figure 5b shows a portion of the ROESY spectrum for a mixture containing 50.0 mM und-Leu, and 50.0 mM Llysine at pH 8.0. The region displayed in Fig. 5b is the same as that displayed in Fig. 5a for the und-Leu: L-arginine mixture. The ROESY spectrum in Fig. 5b shows a strong intramolecular cross peak connecting the und-Leu $H\alpha$ and $H\delta$ resonances and two intermolecular cross peaks connecting the und-Leu Hδ resonances to the L-lysine Hα and HE peaks. However, in the ROESY spectrum of the mixture containing L-lysine, the intermolecular cross peak between the und-Leu H δ and the L-lysine H α resonances is more intense than the corresponding cross peak in the Larginine containing solutions. For example, the ratio of the volumes of the two intermolecular cross peaks is 3.0 in the Fig. 5b spectrum and 5.2 in the Fig. 5a spectrum. Therefore, the ROESY spectra in Fig. 5 suggest that the L-lysine Hα proton and L-lysine primary amine functional group spend more time close to or interacting with the und-Leu micelle surface than the corresponding L-arginine Hα and primary amine. This result, along with the changes observed in the micelle radius with pH in the L-lysinecontaining solutions, suggests that the L-lysine counterions may bind to the und-Leu micelles parallel to the micelle surface with the two positively charged amines acting as a "bridge" between two und-Leu surfactant molecules. This behavior is depicted in Fig. 6b. If the L-lysine bound to the micelles in this manner, we would expect there to be relatively little change in the micelle radii above pH 9.0 when the L-lysine becomes zwitterionic and dissociates from the micelle surface. This behavior is in fact shown in Table 3 and Fig. 4b.

Effect of Amino Acid Chirality on Counterion Binding

Since the surfactant under study and two of the counterions investigated (arginine and lysine) are chiral, the question of whether chirality plays a role in governing the physical properties of the micelles formed by und-Leu and the amino acid counterions was examined. Tables 5 and 6 report diffusion coefficients, fraction bound values, and hydrodynamic radii for und-Leu solutions containing, respectively, D-arginine and D-lysine. These data are plotted in Fig. 4b and d. By comparing these plots to Fig. 4a and c, we can conclude that the chirality of arginine counterion had little to no observable effect on the hydrodynamic radii of the micelles. In other words, experiments with both arginine enantiomers yielded approximately the same size micelles at each pH investigated. Also as observed with L-arginine, at lower pH values the micelle radii are larger when D-arginine was used as the counterion compared to the size of the micelles formed with Na_(ag) counterions. L-Arginine and D-arginine also dissociated from the und-Leu micelle surface beginning at pH 9. Interestingly however, as shown in Fig. 4c and d, the enantiomers of lysine do appear to affect the size of the und-Leu micelles to a small degree with p-lysine forming smaller micelles with an average radius of ca. 10 Å compared to L-lysine which formed micelles with an average radius of ca. 12 Å.

Amide Proton-Solvent Exchange Measurements

In order to gain further insight into the behavior described above, rate constants for the und-Leu NH proton exchange reaction with solvent were measured with an NMR saturation transfer experiment [39]. A stack plot of und-Leu NMR spectra as a function of solution pH is shown in Fig. 7a. Beginning around pH 9.5, the NH resonance begins to decrease in intensity, broaden, and then disappears from the spectrum at pH 11. Figure 7b shows that the NH coupling to the und-Leu alpha proton also disappears at high pH. These changes can be attributed to an increased rate of exchange between the und-Leu NH proton and solvent at high pH [21, 40, 45–50]. If the NH proton exchange with H₂O becomes fast on the NMR time scale at a high pH, its chemical shift becomes the weighted average



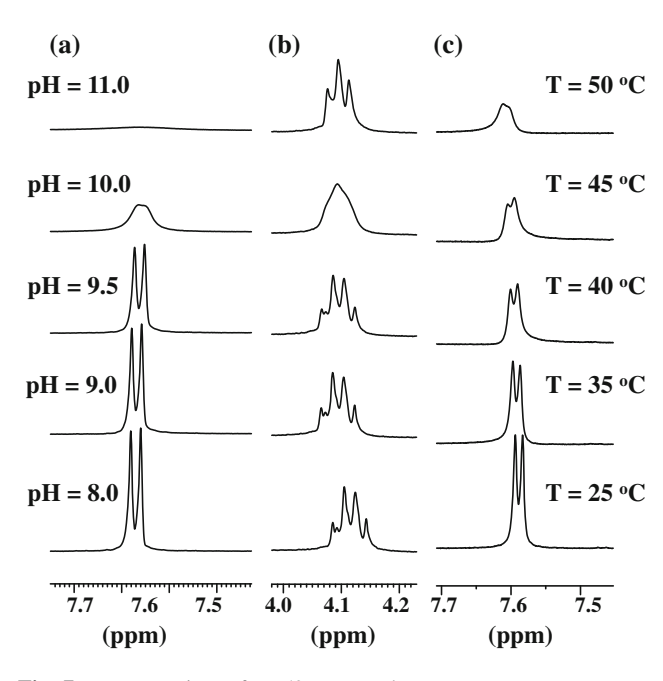


Fig. 7 a NH region of a 50 mM und-Leu NMR spectrum as a function of pH, b H α region of a 50 mM und-Leu NMR spectrum as a function of pH, c NH region of a 50 mM und-Leu NMR spectrum at pH 9.5 as a function of temperature

of the NH and H₂O values. However, the H₂O resonance is much more intense than that of the surfactant NH proton. The average chemical shift of the NH protons undergoing fast exchange would, therefore, be at (or very near) the chemical shift of the solvent, thus causing the NH resonance at 7.6 ppm to disappear. This effect has been observed in peptides and proteins where the rate of amide proton exchange with solvent has been found to change in a similar manner with pH [21, 40, 45–50]. Figure 7c shows changes in the NH region of the und-Leu NMR spectrum at pH 9.5 as a function of temperature. As temperature is increased, the NH resonance is observed to broaden and decrease in intensity in a manner very similar to that shown in Fig. 7a. This observation further suggests that the changes observed in Fig. 7a result from a faster NH proton solvent exchange rate because changes in temperature, which would also be expected to increase the exchange rate, bring about similar changes to those observed when solution pH is increased.

The exchange reaction between amide NH protons and solvent is both base- and acid-catalyzed [21, 40, 45–50]. The rate constant for the amide–solvent exchange reaction $(k_{\rm ex})$ is, therefore, given by Eq. (6), where $k_{\rm OH}$ is the rate constant for the base-catalyzed exchange reaction and $k_{\rm H}$ is the rate constant for the acid-catalyzed exchange reaction [21, 40, 45].

$$k_{\rm ex} = k_{\rm OH} \times \left[{\rm OH}_{\rm (aq)}^{-} \right] + k_{\rm H} \times \left[{\rm H}_3 {\rm O}_{\rm (aq)}^{+} \right]$$
 (8)

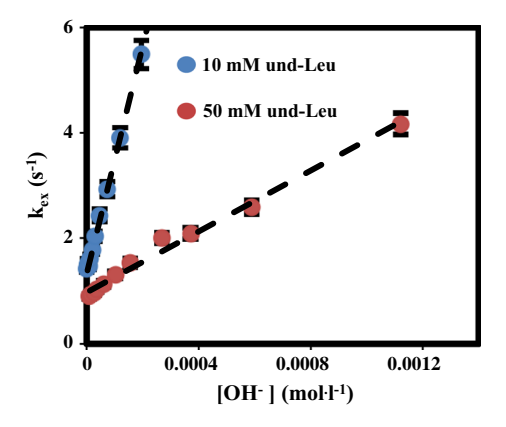
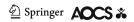


Fig. 8 $k_{\rm ex}$ vs. [OH $^-$] plot for solutions containing 10 mM and 50 mM und-Leu. The slope of each line is $k_{\rm OH}$

At the basic pHs studied here, the second term in Eq. (8) can be assumed to be negligible compared to the first term and Eq. (8) can be written as $k_{\rm ex} = k_{\rm OH} \left[{\rm OH}_{\rm (aq)}^- \right]$. Therefore, if $k_{\rm ex}$ is then measured with the saturation transfer NMR experiment described above, a plot of $k_{\rm ex}$ versus $\left[{\rm OH}^- \right]$ will yield $k_{\rm OH}$ [21, 40, 45–50]. $k_{\rm OH}$ values were measured for und-Leu surfactant solutions at 10.0 mM to establish $k_{\rm OH}$ for the surfactant monomers and then at 50 mM to measure the $k_{\rm OH}$ for the NH protons in micellar form. Figure 8 shows linear plots of $k_{\rm ex}$ versus $\left[{\rm OH}^- \right]$ for both experiments. The slope of each line is $k_{\rm OH}$.

The analysis described above yielded a k_{OH} value of $(2.2 \pm 0.1) \times 10^4 \,\mathrm{M}^{-1} \,\mathrm{s}^{-1}$ for und-Leu surfactant monomers (10 mM) and $(3.4 \pm 0.1) \times 10^3 \,\mathrm{M}^{-1} \,\mathrm{s}^{-1}$ for the und-Leu surfactant in micellar form (50 mM). Rate constants for NH proton-solvent exchange have been used to investigate the conformation of proteins and peptides because of their dependence on both solvent accessibility and hydrogen bond formation [21, 40, 45-50]. In general, NH-solvent exchange rate constants are higher if an NH proton is part of an amino acid on the protein surface where solvent exposure is high and hydrogen bonds with solvent readily form. NH protons that are more shielded from solvent exchange more slowly [21, 40, 45–50]. A similar effect likely explains why the und-Leu k_{OH} value reported above is higher below the CMC and decreases by a factor of ca. 6.5 when the surfactant monomers aggregate into micelles. When a surfactant molecule is part of a micelle, its NH group is less exposed to solvent and as a result the rate of NH exchange with solvent would be expected to be lower than when the surfactant is in monomeric form. It should also be noted that decreased exposure to solvent is not the only effect that can change the rate of NH-solvent exchange and the corresponding $k_{\rm OH}$ value [21, 40, 45–50]. In proteins, if an NH proton forms an intramolecular hydrogen bond with another amino acid, its rate of solvent



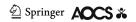
exchange is also decreased [21]. Therefore, H-bonding between surfactant headgoups in the surfactant micelles may also be partially responsible for the decreased $k_{\rm OH}$ values observed above the CMC. Studies are currently underway to determine if similar decreases in NH proton $k_{\rm OH}$ values are observed for other amino acid-based surfactants.

Acknowledgments This work was supported by a National Science Foundation-Research in Undergraduate Institutions (NSF-RUI) Grant (#1213532) to Drs. Fereshteh Billiot and Kevin Morris, a Robert A. Welch Chemistry Departmental Grant to the Chemistry Program at Texas A&M University-Corpus Christi, an NSF CAREER grant (#0449742) to Dr. Eugene Billiot, a Howard University Medicine Alumni Association Endowed Founder's Chair in Basic Science award to Dr. Yayin Fang, and a National Institutes of Health-National Institute on Minority Health and Health Disparities (NIH-NIMHD) Grant (#G12 MD007579) to the RCMI Program at Howard University. We also acknowledge the generosity of the Ralph E. Klingenmeyer family.

References

- Azarmi R, Ashjaran A (2015) Type and application of some common surfactants. J Chem Pharm Res 7:632–640
- Tamrakar S, Darwhekar GN, Sharma R, Mantry P, Soudawat R (2014) Self-emulsifying drug delivery systems: a review of the applicability in drug delivery technologies. ARPB 4:785–790
- Eastoe J, Tabor RF (2014) Surfactants and nanoscience, colloidal foundations of nanoscience. In: Berti D, Palazzo G (eds) Colloidal foundations of nanoscience. Elsevier, Amsterdam
- Felhofer JL, Chumbimuni-Torres KY, Mora MF, Haby GG, Garcia CD (2013) In: Garcia CD, Chumbimuni-Torres KY, Carrilho E (eds) Capillary electrophoresis and microchip capillary electrophoresis: principles, applications, and limitations. Wiley, Hoboken
- Negm NA, Tawfik SM (2013) Environmentally friendly surface active agents and their applications. In: Biresaw G, Mittal KL (eds) Surfactants in tribology. CRC, Boca Raton
- Kumar N, Tyagi R (2014) Applications of dimeric surfactants: a review. J Disper Sci Technol 35:205–214
- Somasundaran P (2012) Self-assembly and self-organization of surfactants in agriculture. Encyclopedia of surface and colloid science 2. CRC, Boca Raton
- Moradi M, Yamini Y (2012) Surfactant roles in modern sample preparation techniques: a review. J Sep Sci 35:2319–2340
- Kamal MS (2016) A review of gemini surfactants: potential application in enhanced oil recovery. J Surfactants Deterg 19:223–236
- Mwangi PM, Rao DN (2014) An overview of surfactants in enhanced oil recovery. In: Romsted LS (ed) Surfactant science and technology. CRC, Boca Raton
- Chandra N, Tyagi VK (2013) Synthesis, properties, and applications of amino acids based surfactants: a review. J Disper Sci Technol 34:800
- Brito RO, Silva S (2011) Enhanced interfacial properties of novel amino acid-derived surfactants: effects of headgroup chemistry and of alkyl chain length and unsaturation. Colloid Surf B 86:65–70
- Bordes R, Tropsch J, Holmberg K (2010) Role of an amide bond for self-assembly of surfactants. Langmuir 26:3077–3083
- Pinazo A, Manresa MA, Marques AM, Bustelo M, Espuny MJ, Perez L (2016) Amino acid-based surfactant: new antimicrobial agents. Adv Colloid Interfac 228:17–39

- Kim SH, Satcher JH, Han TY (2012) Hierarchical ZnO structures templated with amino acid based surfactants. Micropor Mesopor Mat 151:64–69
- Li Y, Holmberg K, Bordes R (2013) Micellization of true amphoteric surfactants. J Colloid Interfac Sci 411:47–52
- Fan H, Han F (2008) Active control of surface properties and aggergation behavior in amino acid-based gemini surfactant systems. J Colloid Intefac Sci 321:227–234
- Bordes R, Holmberg K (2015) Amino acid-based surfactants—do they deserve more attention? Adv Colliod Interfac 222:79–91
- Infante M, Perez L, Pinazo A, Vinardell MP (2004) Amino acidbased surfactants. Green Chem 7:583–592
- Lv J, Qiao W (2015) Unusual pH-regulated surface adsorption and aggregation behavior of a series of asymmetric gemini amino-acid surfactants. Soft Matter 13:2577–2585
- Perrin CL, Chen JH, Ohta BK (1999) Amide proton exchange in micelles. J Am Chem Soc 121:2448–2455
- Perez L, Pinazo A, Pons R, Infante M (2014) Gemini surfactants from natural amino acids. Adv Colloid Interfac 205:134–155
- Billiot FH, McCarroll ME, Billiot EJ, Rugutt JK, Morris KF, Warner IM (2002) Comparison of the aggregation behavior of fifteen polymeric and monomeric dipeptide surfactants in aqueous solution. Langmuir 18:2993–2997
- Stilbs P (1987) Fourier transform pulsed-graident spin-echo studies of molecular diffusion. Prog Nucl Mag Reson Spectrosc 19:1–45
- Willis SA, Stait-Gardner T, Virk AS, Masuda R, Zubkov M, Zheng G, Price WS (2015) Diffusion: definition, description, and measurement. In: Fisher J (ed) Modern NMR techniques for synthetic chemistry. CRC, Boca Raton
- Heisel KA, Goto JJ, Krishnan VV (2012) NMR chromatography: molecular diffusion in the presence of pulsed field gradients in analytical chemistry applications. Am J Anal Chem 3:401–409
- 27. Cohen Y, Avram L, Evan-Salem T, Slovak S, Shemesh N, Frish L (2012) Diffusion NMR in supramolecular chemistry and complex systems. In: Schalley CA (ed) Analytical methods in supramolecular chemistry, 2nd edn. Wiley, Hoboken
- Käerger J (2008) Diffusion measurements by NMR techniques. Mol Sieves 7:85–133
- Stilbs P, Lindman B (1981) Determination of organic counterion binding to micelles through Fourier transform NMR self-diffusion measurements. J Phys Chem 85:2587–2589
- Rashidi-Alavijeh M, Javadian S, Gharibi H, Moradi M, Tehrani-Bagha AR, Shahir AA (2011) Intermolecular interactions between a dye and cationic surfactants: effects of alkyl chain, headgroup, and counterion. Colloid Surf A 380:119–127
- Zuev YF, Gnezdilov OI, Zueva OS, Us'yarov OG (2011)
 Effective self-diffusion coefficients of ions in sodium dodecyl sulfate micellar solutions. Colloid J 73:59–64
- 32. Gnezdilov OI, Zuev YF, Zueva OS, Potarikina KS, Us'yarov OG (2011) Self diffusion of ionic surfactants and counterions in premicellar and micellar solutions of sodium, lithium, and cesium dodecyl sulfates as studied by NMR-diffusometry. Appl Magn Reson 40:91–103
- Deaton K, Feyen E, Nkulabi H, Morris K (2001) Pulsed-field gradient NMR study of sodium dodecyl sulfate micelle-peptide association. Magn Reson Chem 39:276–282
- Begotka BA, Hunsader JL, Oparaeche C, Vincent JK, Morris KF (2006) A pulsed field gradient NMR diffusion investigation of encephalin peptide-dodium dodecyl sulfate micelle association. Magn Reson Chem 44:586–593
- 35. Lipidot Y, Rappoport S, Wolman YJ (1967) Use of esters of *N*-hydroxysuccinimide in the synthesis of *N*-acylamino acids. J Lipid Res 8:142–145
- Kalyanasundaram K, Thomas JK (1977) Environmental effects on vibronic band intensities in pyrene monomer fluorescence and



- their application in studies of micellar systems. J Am Chem Soc 99:2039-2044
- Wu D, Chen A, Johnson CS Jr (1995) An improved diffusion ordered spectroscopy experiment incorporating bipolar gradient pulses. J Magn Reson 115:260–264
- Piotto M, Saudek V, Skienar V (1992) Gradient-tailored excitation for single quantum NMR spectroscopy of aqueous solutions.
 J Biomol NMR 2:661–665
- Forsen S, Hoffman RA (1963) Study of moderately rapid chemical exchange reactions by means of nuclear magnetic double resonance. J Chem Phys 39:2892–2901
- O'Neil JDJ, Sykes BD (1989) NMR studies of the influence of dodecyl sulfate on the amide hydrogen exchange kinetics of a micelle-solubilized hydrophobic tripeptide. Biochemistry 28:699–707
- 41. Lide DR (ed) (2003) CRC handbook of chemistry and physics, 84th edn. CRC, Boca Raton
- Wilkins DK, Grimshaw SB, Receveur V, Dobson CM, Jones JA, Smith LJ (1999) Hydrodynamic radii of native and denatured proteins measured by pulse field gradient NMR techniques. Biochemistry 38:16424–16431
- 43. Berg JM, Tymoczko JL, Gatto GJ Jr, Stryer L (2015) Biochemistry, 8th edn. Freeman, New York
- 44. Bax A, Davis DG (1985) Practical aspects of two-dimensional transverse noe spectroscopy. J Magn Reson 63:207–213
- Narutis VP, Kopple KD (1983) Substrate specificities and structure-activity relationships for acylation of antibiotics catalyzed by kanamycin acetyltransferase. Biochemistry 22:6233–6239
- Lenkinski RE, Stephens RL, Krishna NR (1981) Conformation of angiotensin II: evidence for a specific hydrogen bonded conformation. Biochemistry 20:3122–3126
- 47. Krishna NR, Huang DH, Glickson JD, Rowan R (1979) Amide hydrogen exchange rates of peptide in H₂O solution by ¹H nuclear magnetic resonance transfer of solvent saturation method. Conformations of oxytocin and lysine vasopressin in aqueous solution. Biophys J 26:345–366
- 48. Jamin Y, Eykyn TR, Poon E, Springer CJ, Robinson SP (2014) Detection of the prodrug-activating enzyme carboxypeptidase G2 activity with chemical exchange saturation transfer magnetic resonance. Mol Imaging Biol 16:152–157
- Zheng Z, Brockel C, Ganter B, Lipsick J, Sasaki M, Ogata K, Nishimura Y, Jardetzky O (1996) Amide proton exchange rates in c-Myb DNA binding domain. Quart Magn Reson Biol Med 3:33–45
- Assfalg M, Ragona L, Pagano K, D'Onofrio M, Zanzoni S, Tomaselli S, Molinari H (2016) The study of transient proteinnanoparticle interactions by solution NMR spectroscopy. Biochim Biophys Acta 1864:102–114

Corbin Lewis is an undergraduate research student at Texas A&M Corpus Christi. His research uses NMR and fluorescence spectroscopy and molecular dynamics simulations to characterize amino acid-based surfactants.

Burgoyne H. Hughes is an undergraduate research student at Carthage College. His research uses NMR spectroscopy to characterize counterion binding to amino acid-based surfactants.

Mariela Vasquez is an undergraduate research student at Texas A&M Corpus Christi. Her research involves the synthesis and characterization of amino acid-based surfactants.

Alyssa M. Wall was an undergraduate research student at Carthage College before graduating in 2016. Her research used NMR spectroscopy to characterize the physical properties of amino acid-based surfactants.

Victoria L. Northrup was an undergraduate research student at Carthage College before graduating in 2015. Her research used NMR spectroscopy to investigate the physical properties and dynamics of amino acid-based surfactants.

Tyler J. Wytzleb was an undergraduate research student at Carthage College before graduating in 2016. His research used two-dimensional NMR to investigate counterion binding to amino acid-based surfactants.

Eugene J. Billiot is an associate professor of chemistry at Texas A&M Corpus Christi. His research investigates the factors responsible for chiral recognition with media designed for use as chiral pseudostationary phases in capillary electrophoresis.

Yayin Fang is an associate professor in the Department of Biochemistry and Molecular Biology at Howard University and a HUMAA Endowed Founder's Chair in the Basic Sciences. Her research uses computer modeling to investigate interactions between low molecular weight compounds and targets such as polymers, nucleic acids, and proteins.

Fereshteh H. Billiot is an associate professor of chemistry at Texas A&M Corpus Christi. Her work involves the synthesis of amino acid-based surfactants, their characterization with fluorescence spectroscopy, and their use as chiral selectors in capillary electrophoresis.

Kevin F. Morris is a professor of chemistry at Carthage College. His research uses NMR spectroscopy and molecular dynamics simulations to investigate the structure and dynamics of chiral micelles.

